

MIT Open Access Articles

*Correlation of doping, structure, and
carrier dynamics in a single GaN nanorod*

The MIT Faculty has made this article openly available. **Please share**
how this access benefits you. Your story matters.

Citation: Zhou, Xiang, Ming-Yen Lu, Yu-Jung Lu, Shangjr Gwo, and Silvija Gradec#ak.
"Correlation of doping, structure, and carrier dynamics in a single GaN nanorod." Applied
Physics Letters 102, no. 25 (2013): 253104. © 2013 AIP Publishing LLC

As Published: <http://dx.doi.org/10.1063/1.4812241>

Publisher: American Institute of Physics (AIP)

Persistent URL: <http://hdl.handle.net/1721.1/79628>

Version: Final published version: final published article, as it appeared in a journal, conference
proceedings, or other formally published context

Terms of Use: Article is made available in accordance with the publisher's policy and may be
subject to US copyright law. Please refer to the publisher's site for terms of use.



Correlation of doping, structure, and carrier dynamics in a single GaN nanorod

Xiang Zhou, Ming-Yen Lu, Yu-Jung Lu, Shangjr Gwo, and Silviya Gradečak

Citation: *Appl. Phys. Lett.* **102**, 253104 (2013); doi: 10.1063/1.4812241

View online: <http://dx.doi.org/10.1063/1.4812241>

View Table of Contents: <http://apl.aip.org/resource/1/APPLAB/v102/i25>

Published by the AIP Publishing LLC.

Additional information on Appl. Phys. Lett.

Journal Homepage: <http://apl.aip.org/>

Journal Information: http://apl.aip.org/about/about_the_journal

Top downloads: http://apl.aip.org/features/most_downloaded

Information for Authors: <http://apl.aip.org/authors>

ADVERTISEMENT



Recirculation Pumps *with Speed Control*

Laser Cooling / Chillers
Brushless DC • Magnetic Drive

www.GRIpumps.com/Integrity

GRI
PUMPS
A GORMAN-RUPP COMPANY

Correlation of doping, structure, and carrier dynamics in a single GaN nanorod

Xiang Zhou,¹ Ming-Yen Lu,² Yu-Jung Lu,³ Shangjr Gwo,³ and Silvija Gradečak^{1,a)}

¹*Department of Materials Science and Engineering, Massachusetts Institute of Technology, Cambridge, Massachusetts 02139, USA*

²*Graduate Institute of Opto-Mechatronics, National Chung Cheng University, Min-Hsiung, Chia-Yi 62102, Taiwan*

³*Department of Physics, National Tsing Hua University, Hsinchu 30013, Taiwan*

(Received 19 April 2013; accepted 9 June 2013; published online 26 June 2013)

We report the nanoscale optical investigation of a single GaN p-n junction nanorod by cathodoluminescence (CL) in a scanning transmission electron microscope. CL emission characteristic of dopant-related transitions was correlated to doping and structural defect in the nanorod, and used to determine p-n junction position and minority carrier diffusion lengths of 650 nm and 165 nm for electrons and holes, respectively. Temperature-dependent CL study reveals an activation energy of 19 meV for non-radiative recombination in Mg-doped GaN nanorods. These results directly correlate doping, structure, carrier dynamics, and optical properties of GaN nanostructure, and provide insights for device design and fabrication. © 2013 AIP Publishing LLC. [<http://dx.doi.org/10.1063/1.4812241>]

GaN-based nanostructures are promising materials systems for optoelectronic applications such as high efficiency light emitting diodes^{1,2} (LEDs), and low lasing threshold lasers.^{3–6} These nanowires and nanorods are synthesized by either vapor-liquid-solid mechanism using metal seeds^{7,8} or by catalyst-free approach using plasma assisted molecular beam epitaxy (PAMBE).⁹ Nanoscale correlation of heterostructure properties with the structure, doping, and alloying is essential for improving device design and fabrication. While chemical analyses using energy dispersive x-ray spectroscopy or electron energy loss spectroscopy can precisely determine the position of an alloy junction such as GaN/InGaN, these techniques cannot determine the position of a p-n junction as their sensitivities (0.1–1 at. %) are insufficient to detect dopant concentrations (0.001 at. %). Secondary ion mass spectroscopy (SIMS) typically used to obtain doping profiles in thin films is usually performed on a wafer scale and can only give compositional profile on an ensemble of nanowires of different heights.¹⁰ Other techniques, such as atom probe tomography, electron-beam induced current, or Kelvin probe force microscopy suffer from shortcomings such as challenging sample preparation, requirements for pristine surface conditions, or suitable contacts. Cathodoluminescence in scanning transmission electron microscope (CL-STEM) collects light signal excited by nanometer-sized electron probe, making it suitable to studying optical properties of nanowires,^{11–13} radial,^{14,15} and axial^{16–18} nanowire alloy heterostructures with nanoscale resolution. In addition, physical insights into the correlation of doping, structure, and carrier diffusion can be extracted from CL-STEM optical mapping, particularly in one-dimensional nanostructures. These parameters are critical for future development of nanorod-based devices. For example, shorter minority carrier diffusion lengths have been reported in nanowires compared to bulk in certain materials systems (e.g., GaAs),¹⁹ and increased carrier diffusion through *in-situ* surface

passivation has led to improved performance in GaAs²⁰ and GaAsP²¹ nanowire based solar cells. In this letter, we report on the CL-STEM characterization of a single axial GaN p-n junction nanorod at both room and cryogenic temperatures. Through this method, we not only determine the position of the metallurgical junction but also probe optical transitions associated with dopant energy levels and minority carrier diffusion in a non-destructive and simple manner.

Vertically aligned, catalyst-free GaN p-n junction nanorods were grown using PAMBE on a 3 in., n-type silicon (111) substrate, as reported previously.^{2,4} During the growth, Si was first introduced as n-type dopant, after which Mg was introduced for p-type doping. Wafer-scale SIMS result suggests Mg concentration on the order of 10^{20} cm⁻³.⁴ Single nanorod device exhibits rectifying characteristics in current-voltage measurement at room temperature, confirming the presence of p-n junction.⁴ For TEM and CL-STEM studies, GaN nanorods were mechanically removed from the growth substrate and placed on a carbon film TEM grid. CL-STEM studies on these nanorods were performed using a JEOL 2011 TEM fitted with a Gatan MonoCL3 system using 80 kV electrons with 5 nm, 300 pA probe current. A high sensitivity photomultiplier tube and a CCD camera fitted with 300 line/mm grating were used to detect the CL signal. Besides room temperature (RT) measurements, the sample was cooled by liquid nitrogen for low temperature measurements.

SEM micrograph (Figure 1(a)) shows that GaN nanorods grow perpendicularly to the Si substrate. An inverse tapering is observed in all nanorods, whereas the contrast along nanowire length is indicative of the doping contrast in secondary electron images.²² TEM and selected area electron diffraction results (Figures 1(b) and 1(c)) confirm that the nanorods grow along the $\langle 0001 \rangle$ direction of the wurtzite structure and are approximately 2 μ m long. Figure 1(d) shows TEM Moiré fringes at the base of the nanorod, indicating that coalescence of thinner nanorods occurs during the growth to eventually form bigger nanorods. The top part of the nanorod is single

^{a)}Electronic mail: gradecak@mit.edu

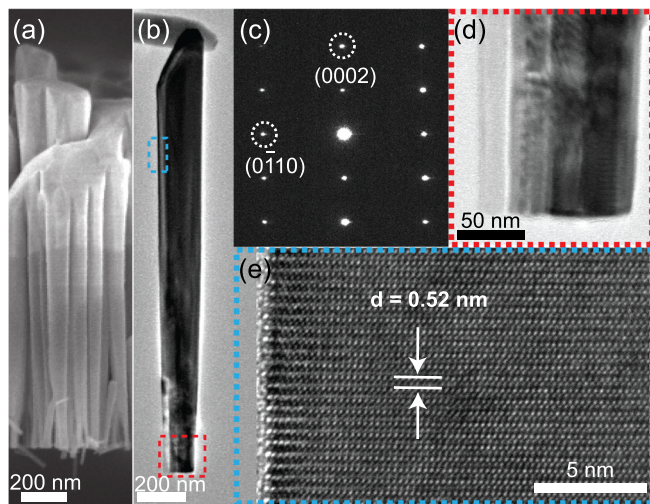


FIG. 1. (a) SEM image of GaN p-n junction nanorods grown on Si substrate. (b) TEM image of a representative GaN p-n junction nanorod. (c) Selected area diffraction of (b) along $[2\bar{1}10]$ zone axis. (d) Higher magnification image of the red-boxed area in (b) showing coalescence of smaller nanorods at the base of the nanorod. (e) Lattice-resolved image taken of the blue boxed area in (b) showing (0001) GaN c -lattice spacing of 0.52 nm.

crystalline without visible defects, as exemplified by the high resolution TEM image in Figure 1(e).

Figures 2(a) and 2(b) show STEM and corresponding panchromatic RT CL images of the same nanorod shown in Figure 1(b). Strong CL emission was observed only in the base portion of the nanorod (nominally Si-doped), whereas the corresponding CL spectrum (Figure 2(d)) reveals the emission peak centered at 3.54 eV (350 nm) with a 190 meV full width at half maximum (FWHM). The observed blue shift of the CL emission compared to the band gap of GaN at

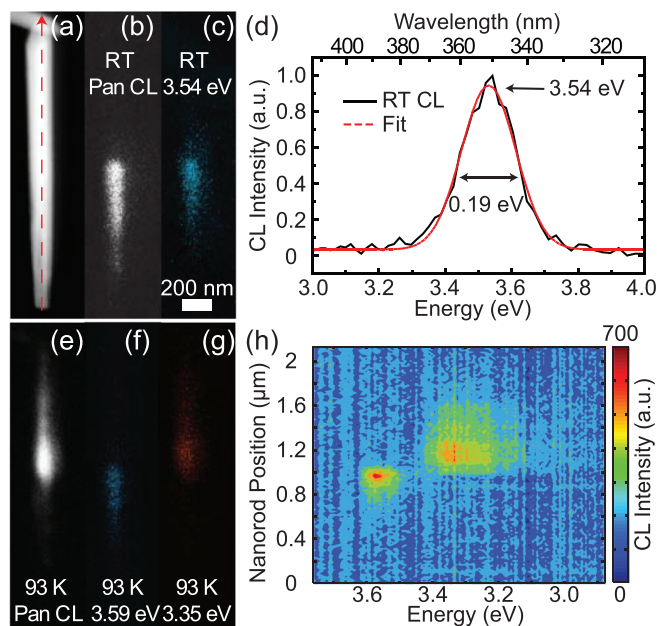


FIG. 2. (a) Dark-field STEM, (b) panchromatic, and (c) 3.54 eV monochromatic CL images of the same nanorod investigated in Figure 1(b), taken at RT. (d) RT CL spectrum (black) showing a peak at 3.54 eV with 190 meV FWHM and the corresponding Gaussian fit (red). (e) Panchromatic, (f) 3.59 eV monochromatic, and (g) 3.35 eV monochromatic CL images of the same nanorod at 93 K. (h) CL spectrum map along the length of the nanorod indicated by the dotted line in (a).

RT (3.4 eV) is likely due to the Burstein-Moss effect,^{23,24} as a high density of carriers is generated in a small volume of the TEM sample. (Based on the experimental conditions, we estimate that the primary electron beam generates $2.9 \times 10^{28} \text{ cm}^{-3} \text{ s}^{-1}$ carrier pairs within the excited volume (see supplemental information²⁵)). A monochromatic image (Figure 2(c)) taken at 3.54 eV confirms that this CL emission comes only from the base portion of the nanorod.

Interestingly, the intensity, energy, and spatial distribution of the CL emission change drastically as temperature is lowered to 93 K. Figure 2(e) shows the panchromatic CL map of the same nanorod shown in Figure 2(a). Clearly, the brightest CL emission at 93 K comes from the top portion of the nanorod, while the base portion, which is bright at RT, exhibits a drastically reduced CL luminescence compared to the top portion. Moreover, a CL line scan spectrum image (Figure 2(h)) along the nanorod length reveals distinct emission in different nanowire parts. The CL spectrum from the base portion of the nanorod consists mainly of a relatively sharp peak centered at 3.59 eV (345 nm). In contrast, the CL emission from the top portion is dominated by an asymmetrical broad emission with the peak intensity at 3.35 eV (350 nm), with a long tail comprising of phonon replicas spaced out by 92 meV LO phonons²⁶ (see supplemental information²⁵ for individual spectra). The pair of monochromatic images taken at 3.59 eV and 3.35 eV (Figures 2(f) and 2(g), respectively) confirms that the two portions of the nanorods exhibit different, well-defined CL emission at 93 K.

The observed spatial distribution and spectral response of the CL signal from the two parts of the nanorod are indicative of its doping. For the base portion of the nanorod, CL peak at 93 K is only slightly blue shifted (0.05 eV) with respect to the peak at RT implying they have the same origin. The positions and relatively narrow widths of the peak suggest that it originates from either a near band edge transition or a shallow donor level. The 3.35 eV peak produced by the top part of the nanowire is typical of an optical transition associated with unionized Mg acceptor.^{27–31} The spectral analysis and the mapping results indicate that the top portion of the nanorod is p-doped by Mg, conversely the base portion is n-doped by Si. Furthermore, by comparing the energy level of the near band edge emission and conduction band to Mg level transition, we can estimate that the acceptor level in the Mg-doped GaN is located about 0.24 eV above the valence band, a value consistent with the reported values (0.18–0.25 eV) for Mg-doped GaN thin films.^{27–32}

The observation that the p-type GaN section has much higher CL intensity at 93 K than at RT can be quantitatively explained considering Mg acceptor ionization. With an acceptor level of 0.24 eV, Mg concentration of 10^{20} cm^{-3} , and average effective hole mass of $1.4 m_0$,²⁶ the number of thermally activated acceptors can be estimated using Fermi-Dirac statistics. Our calculations show a near five order of magnitude (from 10^{17} cm^{-3} to 10^{12} cm^{-3}) decrease in the number of ionized acceptors from 300 K to 93 K, and conversely, a significant increase in the concentration of unionized Mg acceptor levels leading to a sharp increase in intensity of acceptor-related optical transition at low temperatures.

GaN nanorods with incorporated p-n junctions could be made into photodetectors, LEDs, and lasers. Knowing the

position of the metallurgical junction during the nanorod growth is crucial for device design and fabrication to improve the device performance. From the CL line scan spectrum mapping with 16 nm steps, we can further infer the position of the metallurgical p-n junction by closely analyzing the integrated intensity profile (Figure 3) of the near band edge luminescence (3.59 eV) and acceptor level related luminescence (3.35 eV). We observe that the intensity of the 3.59 eV peak from n-type GaN begins to rise from the base of the nanorod, reaches a maximum at $0.95 \mu\text{m}$ and drops down to zero at approximately $1.2 \mu\text{m}$. The intensity of the 3.35 eV p-type CL emission shows a sharp rise at approximately $0.8 \mu\text{m}$, reaches a maximum at $1.09 \mu\text{m}$, and begins a more gradual decline until the top of the nanorod. Based on the intensity profile, we can deduce that the doping switches from n-type to p-type in a 140 nm section between $0.95 \mu\text{m}$ and $1.09 \mu\text{m}$ from the base of the nanorod. Here, we note that the observed 140 nm overlap is not due to the beam broadening as the Monte-Carlo simulation of electron-matter interaction using WINCASINO software³³ shows that 95% of energy transfer from the incident electron beam occurs within 5 nm radius of the incidence of the sample. We cannot rule out the possibility of limited Si and Mg interdiffusion, which has been reported in p-GaN growth using metalorganic chemical vapor deposition^{34,35} performed at temperatures above 1000°C . However, p-n junction nanorods investigated here were grown at 800°C so dopant diffusivity is much lower in our case. Studies on Mg diffusion in PAMBE-grown GaN thin films also shows insignificant Mg diffusion compared to the observed 140 nm overlap of the CL intensities.^{36,37} Since the effects of electron-matter interaction volume and dopant diffusion are small, we attribute the overlapping of the CL intensities to carrier diffusion inside the nanorod. When the electron beam is positioned in the Si-doped region close to the metallurgical junction, some of the generated carriers can diffuse to the p-doped region where they recombine, resulting in a decrease in 3.59 eV CL intensity and a 3.35 eV CL emission intensity tail. Based on the symmetry of the CL intensity decline, we define the position of the p-n junction at the crossing point of the CL

intensity profiles, which is $1.03 \mu\text{m}$ from the base of the nanorod. This position also approximately coincides with the 50% point of the CL intensities.

In this analysis, we did not take into account charge separation in the depleted p-n junction that would result in a decrease in the CL intensities when the electron beam scans inside the depleted p-n junction, as observed in a SEM-CL study on a ZnO nanowire Schottky junction.³⁸ Such a dark area in the middle section of the nanorod was not observed in our case. One important difference between our CL study and the work in Ref. 28 is that the nanorods we investigated are suspended on an amorphous carbon film instead of contacted to an external circuit. As a result, even if charge separation occurs inside the junction, there will be significant charge build up at both ends of the nanorod with a direction and magnitude that cancels out the junction build-in field. This scenario is likely to occur based on the above mentioned generation rate and the fact that the intrinsic concentration of GaN at 93 K is negligible. The CL intensity profiles of the n- and p-doped GaN optical transitions would thus be purely due to doping and carrier diffusion, with minimal effect from build-in potential and carrier drift inside the junction.

Besides the CL intensity variation due to doping in the middle of the nanorod, decrease in the CL intensity near the base and the top of the nanorod are also observed in Figure 3. For the n-GaN section, the quenching of CL emission could be related to the structural defects during nanorod coalescence. In Figure 1(c), we show that the base of the nanorod consists of several thin rods that coalesce at about 450 nm into the nanorod. This length scale is consistent with the length of the n-GaN section with low CL emission. Indeed, detailed TEM studies on MBE grown GaN nanorods have shown the presence of defects such as small angle grain boundaries, dislocations, and stacking faults when thinner GaN nanorods coalesce.^{9,39} These defects have been observed in epitaxial lateral overgrown GaN thin films and are known to be non-radiative recombination centers that quench CL emission.⁴⁰⁻⁴³ Charge carriers generated by the electron beam within the diffusion length from the defects can recombine non-radiatively, resulting in quenching of the CL signal. Carriers generated far away from the base are less likely to diffuse into the defect region, thus, the CL signal increases when the electron beam is scanned toward the middle of the nanorod (away from the defects). Since the intensity of the CL emission is mostly governed by the concentration of minority carriers, we can then fit decay of the CL intensity towards the base of the nanorod as an exponential decay function: $I = a \exp(\pm(x - b)/L_{e,h}) + I_0$, where I is the CL intensity, L_e and L_h are electron and hole diffusion lengths as minority carriers, respectively, a , b , and I_0 are fitting constants. In this way, we estimated the minority diffusion length of holes in n-GaN at 93 K to be $L_h = 165 \pm 10 \text{ nm}$, which is comparable to the values reported in n-GaN thin films and nanowires measured by different techniques.⁴⁴⁻⁴⁷ The intensity of p-GaN emission (3.35 eV) also decreases towards the tip of the nanorod, which suggests the presence of other non-radiative recombination centers near the tip the nanorod not revealed by TEM studies. By applying the similar approach, we extract the electron diffusion length in p-GaN

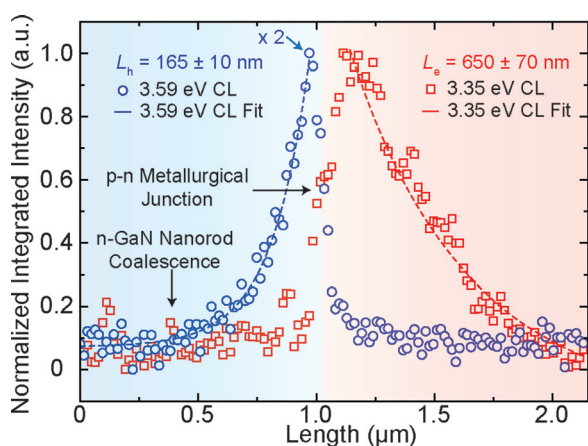


FIG. 3. Normalized integrated intensities of the 3.59 eV and 3.35 eV CL luminescence along the length of the nanorod shown in Figure 2(h). The positions of the nanorod coalescence in the n-GaN section and metallurgical junction are indicated. The squares and circles are experimental data, and the dashed lines are fits based on an exponential decay model.

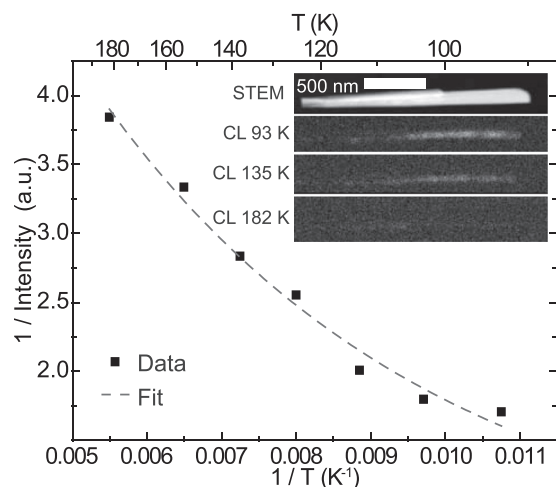


FIG. 4. CL intensity as a function of temperature for a GaN nanorod from 93 K to 185 K. (Experimental data in squares and fitting in dashed line.) Insets show the STEM and corresponding CL images used to extract the data.

to be $L_e = 650 \pm 70$ nm at 93 K. The minority carrier diffusion length, while important for optoelectronic device design, is also an indicator of material quality. In GaN thin films, minority carrier diffusion lengths are limited by the density of dislocations.^{45,48} For the nanorod investigated, minority carrier diffusion length in n-GaN is limited by defects caused by thinner nanorod coalescence. In the p-GaN nanorod portion, while no visible defects were observed, the electron diffusion is likely to be limited by surface recombination. These results provide an important insight for the design and fabrication of optoelectronic devices using nanowires and nanorods as building blocks. For example, minority carrier diffusion length is one of the key factors in the figure of merit of photodetectors to optimize sensitivity and speed.

Finally, we also measured the intensity of the GaN CL emission as a function of temperature to further investigate the phenomenon of thermally activated CL quenching. Panchromatic images of a single GaN p-n junction nanorod were taken in the 93–182 K temperature range, and the CL intensity from the p-GaN region was measured (Figure 4). Following the treatment of Leroux *et al.*,²⁷ the quenching of the CL intensity I with respect to temperature is caused by thermally activated non-radiative recombination centers: $I = I_0 / (1 + \alpha \exp(-E_a/kT))$, where I_0 is total number of carrier pairs excited, α is proportional to the non-radiative recombination time, and E_a is the activation energy for non-radiative recombination. By fitting the experimentally obtained results shown in Figure 4, the activation energy of $E_a = 19 \pm 5$ meV was extracted. For the n-GaN region, the CL intensity remains low throughout the temperature range and a reliable temperature-dependent study is not achievable. Given that no visible defects are observed in the p-GaN section, the non-radiative recombination centers likely originate from surface states, which also limit minority carrier diffusion lengths discussed previously. Proper surface passivation for both bulk and nanostructured GaN can reduce surface states density and improve minority carrier diffusion⁴⁴ and light emission.^{49,50}

In conclusion, using CL-STEM, we identified the position of a p-n junction with high spatial resolution inside a

single GaN nanorod. The overlap of the CL signals from n- and p-doped GaN was shown to be limited only by carrier diffusion. Si doped n-GaN exhibits near band edge CL emission at both room and cryogenic temperature, while Mg-doped p-GaN emits light strongly only at cryogenic temperatures due to temperature-dependent dopant ionization. We confirmed that the Mg acceptor level is 240 meV above the valence band by comparing the CL spectra of n- and p-type GaN sections. In addition, CL quenching along the length of the nanorod was attributed to structural defects through a combination of TEM and CL-STEM investigations. The minority carrier diffusion lengths were determined to be 165 ± 10 nm and 650 ± 70 nm for n- and p-type GaN, respectively. Temperature-dependent studies on CL intensity further revealed a thermally activated non-radiative recombination center with the activation energy of 19 meV in p-GaN. The measured optical emission, dopant level, and estimated carrier diffusion lengths from this study focusing on GaN nanorods are consistent with the previous thin film studies. The defect induced CL quenching highlights the importance of controlling nanorod coalescence during MBE growths and surface passivation for nanostructures to further improve the performance of devices made from these nanostructures.

This work was funded by the Center for Excitonics, Energy Frontier Research Center funded by the U.S. Department of Energy, Office of Basic Energy Sciences under Award No. DE-SC0001088. The authors acknowledge the use of the MRSEC Shared Experimental Facilities at MIT, supported by the National Science Foundation under Award No. DMR-08-19762. M. Lu, Y. Lu, and S. Gwo also acknowledge support from the National Science Council (NSC) in Taiwan (NSC 101-2218-E-194-002 and NSC-101-2628-M-007-006). We would like to thank Dr. Yong Zhang and Dr. Shiahn Chen for their technical assistance, and Dr. Filippo Fabbri for useful discussions.

¹F. Qian, S. Gradečak, Y. Li, C. Y. Wen, and C. M. Lieber, *Nano Lett.* **5**, 2287 (2005).

²H. W. Lin, Y. J. Lu, H. Y. Chen, H. M. Lee, and S. Gwo, *Appl. Phys. Lett.* **97**, 073101 (2010).

³S. Gradečak, F. Qian, Y. Li, H. G. Park, and C. M. Lieber, *Appl. Phys. Lett.* **87**, 173111 (2005).

⁴Y. J. Lu, H. W. Lin, H. Y. Chen, Y. C. Yang, and S. Gwo, *Appl. Phys. Lett.* **98**, 233101 (2011).

⁵Y. J. Lu, J. Kim, H. Y. Chen, C. H. Wu, N. Dabidian, C. E. Sanders, C. Y. Wang, M. Y. Lu, B. H. Li, X. G. Qiu, W. H. Chang, L. J. Chen, G. Shvets, C. K. Shih, and S. Gwo, *Science* **337**, 450 (2012).

⁶F. Qian, Y. Li, S. Gradečak, H. G. Park, Y. J. Dong, Y. Ding, Z. L. Wang, and C. M. Lieber, *Nature Mater.* **7**, 701 (2008).

⁷S. K. Lim, S. Crawford, and S. Gradečak, *Nanotechnology* **21**, 345604 (2010).

⁸X. Zhou, J. Chesin, S. Crawford, and S. Gradečak, *Nanotechnology* **23**, 285603 (2012).

⁹H. Y. Chen, H. W. Lin, C. H. Shen, and S. Gwo, *Appl. Phys. Lett.* **89**, 243105 (2006).

¹⁰A. C. E. Chia, J. P. Boulanger, and R. R. LaPierre, *Nanotechnology* **24**, 045701 (2013).

¹¹M. M. Brewster, M. Y. Lu, S. K. Lim, M. J. Smith, X. Zhou, and S. Gradečak, *J. Phys. Chem. Lett.* **2**, 1940 (2011).

¹²M. M. Brewster, X. Zhou, S. K. Lim, and S. Gradečak, *J. Phys. Chem. Lett.* **2**, 586 (2011).

¹³M. M. Brewster, X. Zhou, M. Y. Lu, and S. Gradečak, *Nanoscale* **4**, 1455 (2012).

- ¹⁴S. K. Lim, M. Brewster, F. Qian, Y. Li, C. M. Lieber, and S. Gradečak, *Nano Lett.* **9**, 3940 (2009).
- ¹⁵F. Qian, M. Brewster, S. K. Lim, Y. C. Ling, C. Greene, O. Laboutin, J. W. Johnson, S. Gradečak, Y. Cao, and Y. Li, *Nano Lett.* **12**, 3344 (2012).
- ¹⁶G. Tourbot, C. Bougerol, F. Glas, L. F. Zagonel, Z. Mahfoud, S. Meuret, P. Gilet, M. Kociak, B. Gayral, and B. Daudin, *Nanotechnology* **23**, 135703 (2012).
- ¹⁷L. F. Zagonel, L. Rigutti, M. Tchernycheva, G. Jacopin, R. Songmuang, and M. Kociak, *Nanotechnology* **23**, 455205 (2012).
- ¹⁸L. F. Zagonel, S. Mazzucco, M. Tence, K. March, R. Bernard, B. Laslier, G. Jacopin, M. Tchernycheva, L. Rigutti, F. H. Julien, R. Songmuang, and M. Kociak, *Nano Lett.* **11**, 568 (2011).
- ¹⁹C. C. Chang, C. Y. Chi, M. Q. Yao, N. F. Huang, C. C. Chen, J. Theiss, A. W. Bushmaker, S. LaLumondiere, T. W. Yeh, M. L. Povinelli, C. W. Zhou, P. D. Dapkus, and S. B. Cronin, *Nano Lett.* **12**, 4484 (2012).
- ²⁰G. Mariani, A. C. Scofield, C. H. Hung, and D. L. Huffaker, *Nat. Commun.* **4**, 1497 (2013).
- ²¹J. V. Holm, H. I. Jorgensen, P. Krogstrup, J. Nygard, H. Y. Liu, and M. Aagesen, *Nat. Commun.* **4**, 1498 (2013).
- ²²I. Volotsenko, M. Molotskii, Z. Barkay, J. Marczewski, P. Grabiec, B. Jaroszewicz, G. Meshulam, E. Grunbaum, and Y. Rosenwaks, *J. Appl. Phys.* **107**, 014510 (2010).
- ²³Y. H. Yang, X. Y. Chen, Y. Feng, and G. W. Yang, *Nano Lett.* **7**, 3879 (2007).
- ²⁴E. Oh, B. W. Lee, S. J. Shim, H. J. Choi, B. H. Son, Y. H. Ahn, and L. S. Dang, *Appl. Phys. Lett.* **100**, 153110 (2012).
- ²⁵See supplementary material at <http://dx.doi.org/10.1063/1.4812241> for estimation of electron induced carrier density in the nanorod, and detailed CL spectra of n- and p-GaN nanorod portions at 93 K.
- ²⁶H. Morkoç, *Handbook of Nitride Semiconductors and Devices* (Wiley-VCH Verlag GmbH & Co. KGaA, Weinheim, 2009), p. 18.
- ²⁷M. Leroux, N. Grandjean, B. Beaumont, G. Nataf, F. Semond, J. Massies, and P. Gibart, *J. Appl. Phys.* **86**, 3721 (1999).
- ²⁸S. Fischer, C. Wetzel, E. E. Haller, and B. K. Meyer, *Appl. Phys. Lett.* **67**, 1298 (1995).
- ²⁹B. Monemar, *J. Cryst Growth* **189/190**, 1 (1998).
- ³⁰F. Mireles and S. E. Ulloa, *Phys. Rev. B* **58**, 3879 (1998).
- ³¹M. Ilegems and R. Dingle, *J. Appl. Phys.* **44**, 4234 (1973).
- ³²M. Smith, G. D. Chen, J. Y. Lin, H. X. Jiang, A. Salvador, B. N. Sverdlov, A. Botchkarev, H. Morkoç, and B. Goldenberg, *Appl. Phys. Lett.* **68**, 1883 (1996).
- ³³R. Gauvin, E. Lifshin, H. Demers, P. Horny, and H. Campbell, *Microsc. Microanal.* **12**, 49 (2006).
- ³⁴Y. L. Chang, M. Ludowise, D. Lefforge, and B. Perez, *Appl. Phys. Lett.* **74**, 688 (1999).
- ³⁵R. Gutt, K. Köhler, J. Wiegert, L. Kirste, T. Passow, and J. Wagner, *Phys. Status Solidi C* **8**, 2072 (2011).
- ³⁶I. P. Smorchkova, E. Haus, B. Heying, P. Kozodoy, P. Fini, J. P. Ibbetson, S. Keller, S. P. DenBaars, J. S. Speck, and U. K. Mishra, *Appl. Phys. Lett.* **76**, 718 (2000).
- ³⁷S. Guha, N. A. Bojarczuk, and F. Cardone, *Appl. Phys. Lett.* **71**, 1685 (1997).
- ³⁸J. S. Hwang, F. Donatini, J. Pernot, R. Thierry, P. Ferret, and L. S. Dang, *Nanotechnology* **22**, 475704 (2011).
- ³⁹K. A. Grossklau, A. Banerjee, S. Jahangir, P. Bhattacharya, and J. M. Millunchick, *J. Cryst Growth* **371**, 142–147 (2013).
- ⁴⁰M. A. L. Johnson, Z. H. Yu, J. D. Brown, N. A. El-Masry, J. W. Cook, and J. F. Schetzina, *J. Electron. Mater.* **28**, 295 (1999).
- ⁴¹P. Corfdir, D. Simeonov, E. Feltin, J. F. Carlin, P. Lefebvre, N. Grandjean, B. Deveaud-Pledran, and J. D. Ganiere, *Phys. Status Solidi C* **8**, 1394 (2011).
- ⁴²B. J. Ryan, D. P. Lowney, M. O. Henry, P. J. McNally, E. McGlynn, K. Jacobs, and L. Considine, *Thin Solid Films* **473**, 308 (2005).
- ⁴³S. Dassonneville, A. Amokrane, B. Sieber, J. L. Farvacque, B. Beaumont, V. Bousquet, P. Gibart, K. Leifer, and J. D. Ganiere, *Physica B* **273–274**, 148 (1999).
- ⁴⁴L. Baird, C. P. Ong, R. A. Cole, N. M. Haegel, A. A. Talin, Q. M. Li, and G. T. Wang, *Appl. Phys. Lett.* **98**, 132104 (2011).
- ⁴⁵Z. Z. Bandic, P. M. Bridger, E. C. Piquette, and T. C. McGill, *Appl. Phys. Lett.* **72**, 3166 (1998).
- ⁴⁶M. Niehus and R. Schwarz, *Phys. Status Solidi C* **3**, 2103 (2006).
- ⁴⁷D. G. Zhao, D. S. Jiang, H. Yang, J. J. Zhu, Z. S. Liu, S. M. Zhang, J. W. Liang, X. P. Hao, L. Wei, X. Li, X. Y. Li, and H. M. Gong, *Appl. Phys. Lett.* **88**, 252101 (2006).
- ⁴⁸K. Kumakura, T. Makimoto, N. Kobayashi, T. Hashizume, T. Fukui, and H. Hasegawa, *Appl. Phys. Lett.* **86**, 052105 (2005).
- ⁴⁹T. Maruyama, K. Yorozu, T. Noguchi, Y. Seki, Y. Saito, T. Araki, and Y. Nanishi, *Phys. Status Solidi C* **0**, 2031 (2003).
- ⁵⁰C. Huh, S. W. Kim, H. S. Kim, I. H. Lee, and S. J. Park, *J. Appl. Phys.* **87**, 4591 (2000).